Modeling Equatorial Annual Cycle with a Linear Coupled Model

ZHENGYU LIU

Department of Atmospheric and Oceanic Sciences, University of Wisconsin—Madison, Madison, Wisconsin

(Manuscript received 21 July 1995, in final form 2 January 1996)

ABSTRACT

A simple linear coupled ocean–atmosphere model is used to study the equatorial annual cycle. The ocean is a slab mixed-layer model and the atmosphere is the Lindzen–Nigam model. The model is shown to capture most features of the observed equatorial annual cycle. A significant part of the tropical annual cycle is found to be generated by the extratropical annual variability that propagates toward the equator through a coupled ocean–atmosphere wave. The back-pressure effect in the atmosphere model can contribute to several important aspects of the variability, especially in the vicinity of the equator. Comparison with other mechanisms for the equatorial annual cycle is also discussed.

1. Introduction

Annual variability in the eastern equatorial Pacific has received increasing attention in recent years (Horel 1982; Mitchell and Wallace 1992; Wang 1994). One important reason is that the annual variability seems to play an important role in interannual climate variability (Jin et al. 1994; Tziperman et al. 1994; Chang et al. 1994). Despite its importance, a correct simulation of the equatorial annual variability still remains a challenging task for fully coupled ocean–atmosphere models (Mechoso et al. 1995). Part of the reason is our poor understanding of the origin of the equatorial annual cycle. The sun crosses the equator twice a year, resulting in a local solar radiation dominated by the semi-annual cycle over the equator. Thus, the pure local radiation forcing can not account for the observed equatorial annual cycle.

Several recent works have shed light on the mechanism for the formation of the equatorial annual cycle. Two principles seem to be well accepted (Mitchell and Wallace 1992; Chang and Philander 1994; Liu and Xie 1994; Li and Philander 1996, unpublished manuscript). First, ocean–atmosphere interaction is crucial for the annual cycle. Second, certain asymmetry is necessary in the climatological state (including the basin geometry) to generate the annual variability on the equator from the annual harmonic of solar radiation that is mostly antisymmetric about the equator.

Specific mechanisms of the annual variability, however, are still intensive research topics. The observations of Mitchell and Wallace (1992) and the theoretical study of Chang and Philander (1994) suggest that the annual cycle may be triggered by the North America monsoon and can be further amplified by the coupled instability between the meridional wind and equatorial upwelling. A further model study by Li and Philander shows that the annual cycle can also be enhanced significantly by other factors such as evaporation and low-level stratus clouds. These studies emphasize the role of coupled equatorial instability. They also tend to focus locally on the feature of the annual variability on the equator.

An alternative view is proposed by Liu and Xie (1994, hereafter LX). It is proposed that a substantial part of the equatorial annual variability can be generated by the propagation of extratropical annual variability towards the equator. The propagation is mainly accomplished by a coupled ocean–atmosphere wave that is caused by the wind–evaporation-mixing feedback between the boundary-layer atmosphere and ocean. This view is strongly motivated by two observations of the equatorial annual cycle: first, it has a broad meridional structure; second, it exhibits a rapid phase propagation from the Southern Hemisphere toward the equator (Fig. 1 of LX; Wang 1994). Furthermore, LX is also strongly motivated by the fact that large annual variability exists in the extratropics due to the local solar radiation there. Although weak at the equator, the solar radiation reaches to over 50 W m^2 at 20° of latitude (Reed 1977), which is strong enough to generate a local annual variability of more than 1°C in the surface mixed layer. Thus, the equatorial annual cycle can be thought as a "forced-mode" that responds to the extratropical annual variability. If the forced response is true, one should be able to model the major

Corresponding author address: Dr. Z. Liu, Department of Atmospheric and Oceanic Sciences, University of Wisconsin—Madison, Madison, WI 53706-1695.
E-mail: znl@ocean.meteor.wisc.edu

features of the equatorial annual cycle with a linear coupled ocean–atmosphere model.

It is important to point out that the forced response view of LX is in sharp contrast to that for the El Niño/Southern Oscillation (ENSO). The ENSO has to be dominated by a "free-mode" within the ocean–atmosphere system because anywhere on the earth there is no solar radiation forcing at the frequency of ENSO. Furthermore, nonlinearity (e.g., Suarez and Schopf 1988) is necessary in order to balance initial linear instability to achieve a finite amplitude of oscillation.

Liu and Xie has shown that a linear coupled model can indeed simulate many gross features of the annual variability successfully. However, it has one major unrealistic feature: the annual variability, especially the wind field, is poorly simulated in the vicinity (say, within 5°) of the equator. One obvious reason is the lack of the "back-pressure" effect (BP) in the atmosphere model (Lindzen and Nigam 1987). Therefore, part of our goal is to improve the simulation of the annual variability by including the BP effect.

The inclusion of the BP enables the atmosphere to respond to nonlocal sea surface temperature (SST) anomaly. This may alter the propagation feature of the coupled wave of LX significantly because it depends mainly on the atmospheric response to the local SST gradient. Therefore, the other part of our goal is to investigate how well the equatorward propagation mechanism works in the presence of BP?

Our conclusion is that the inclusion of the BP is able to improve our simulation of annual cycle significantly, especially in the vicinity of the equator. At the same time, it does not change the propagation feature dramatically especially outside, say, 5° of the equator. This can be understood physically as follows. The BP effect mainly corrects the atmospheric wind in the vicinity of the equator. Therefore, BP can improve the coupled model results in the vicinity of the equator without distorting the coupled model results away from the equator significantly. The paper is arranged as follows. Section 2 introduces the model. The simulation of the annual cycle is described in section 3. A summary and further discussions are presented in section 4.

2. The model

Both of our ocean and atmosphere models are boundary-layer models and are the same as those in LX, except for the inclusion of the BP in the Lindzen–Nigam atmosphere model (1987). All the equations are linearized perturbation equations and the reader should refer to LX for more details of the derivation. The equations will be written here in Cartesian coordinate. But in the numerical results presented, the equations are solved in the spherical coordinate.

The atmosphere model is the Lindzen–Nigam model, in the form presented by Neelin (1989).

$$-fV = -\partial_x\left(\psi - \frac{C_0^2}{2T_0}T\right) - D_m U, \quad (2.1a)$$

$$fU = -\partial_y\left(\psi - \frac{C_0^2}{2T_0}T\right) - D_m V, \quad (2.1b)$$

$$\frac{\psi}{\tau} + C_0^2(\partial_x U + \partial_y V) = 0, \quad (2.1c)$$

where f is the Coriolis parameter, (U, V) are anomalous surface winds, T is the SST anomaly, $1/D_m$ is the atmospheric momentum damping time, $C_0 = (\sqrt{g\bar{H}_a})^{1/2}$ is the gravity wave speed in the cumulus boundary layer that has a thickness of H_a, and τ is the adjustment time scale for the BP, which depends on the boundary-layer cumulus convection. The difference from the model of LX is the finite adjustment time τ that allows the BP to exist in the present model. The values of the parameters for the standard runs are similar to Lindzen and Nigam and are given in Table 1.

The ocean model is a slab mixed-layer model. The linearized sea surface temperature (SST) equation can be written as (see LX)

$$(\partial_t + d_T + \bar{u}\partial_x + \bar{v}\partial_y)T + u\partial_x\bar{T} + v\partial_y\bar{T} = \frac{2}{\rho_0 c_p h}\left[Q - \left(1 + \frac{3h_E}{2h}\right)\bar{Q}_E\frac{\bar{U}U + \bar{V}V}{\bar{U}^2 + \bar{V}^2}\right] + d_L\nabla^2 T. \quad (2.2)$$

Here $\bar{}$ represents the annual-mean field, Q is the anomalous shortwave radiation heating, $\bar{Q}_E$ is the mean evaporation cooling, h is the mixed-layer depth, $1/d_T$ is the Newtonian damping time for a SST anomaly, and h_E is a pseudo evaporation *Monin–Obukov* ocean depth due to the evaporation. A Laplace diffusion term is also added. Finally, in the surface mixed layer, the momen-

TABLE 1. Standard parameters used in the calculation.

Parameter	Meaning	Control
	Atmosphere	
$1/D_m$	Momentum damping time	2×10^5 s
τ	BP adjustment time	1800 s
C_0	Gravity wave speed	150 m s^{-1}
	Ocean	
c_p	Heat capacity	4×10^3 J(kg)$^{-1}$ K^{-1}
ρ_0	Density of water	10^3 (kg) m^{-3}
h_E	Pseudo evaporation M-O depth	50 m
$\bar{Q}_E$	Mean evaporation heat flux	60 W m^{-2}
$1/d_T$	SST damping time	0.5×10^7 s
$1/d_m$	Current damping time	0.5×10^6 s
d_L	Diffusive coefficient	10^7 cm s^{-2}
Δ_T	Thermocline temperature difference	
	Land	
C_{PL}		5 K/(100 W m^{-2})
	Coupling	
γ	Wind-forcing coefficient	2×10^{-7} s^{-1}
T_0	Reference temperature	293 K

tum equations for anomalous ocean currents are simply the wind-driven balance:

$$-fv = \gamma U - d_m u, \tag{2.3a}$$

$$fu = \gamma V - d_m v, \tag{2.3b}$$

where γ is the wind forcing coefficient. The values of the standard parameters are given in Table 1. As in LX, Eqs. (2.3a,b) are also used for the calculation of the mean current in the SST Eq. (2.2). Although crude, this is a simple approach with certain consistency within our model.

Equations (2.1)–(2.3) form a set of linear coupled ocean–atmosphere model. This model will be shown to be able to capture the major features of the equatorial annual cycle. The critical term is the wind anomaly term—the second term on the right-hand side of the SST Eq. (2.2). This term is caused by two comparable effects: the wind speed variation on both the ocean mixed-layer entrainment and the surface evaporation. Hereafter, we will refer to this term as the wind-evaporation–mixing term. This term has been found important in affecting SST in the equatorial ocean (Xie 1994).

In the absence of BP [i.e., $\tau = 0$ and therefore $\psi = 0$ in Eqs. (2.1a,b,c)], the atmospheric response to SST gradient is local. The coupled model can be reduced to a single first-order partial differential equation in terms of SST [see Eq. (3.3) of LX]. This equation shows clearly the nondispersive coupled wave that propagates both zonally and meridionally. As discussed by LX (see their Fig. 3 and the discussion), for realistic parameters, the wind evaporation–mixing effect is the most important for wave propagation. Under a mean easterly wind, the perturbation propagates rapidly equatorward and westward. Adding a mean equatorward wind enhances the equatorward propagation but slows down the westward propagation near the equator. The further addition of a mean southerly wind across the equator tends to sweep the disturbance to the north of the equator.

With BP, the model can no longer be reduced to a single equation. However, the propagation feature is still similar to the case without BP. One example is shown in Fig. 1. The solar radiation forcing and all the mean field in the SST Eq. (2.2) are set to zero except for a mean easterly trade wind. The initial condition is a pair of elliptic-shaped positive SST anomalies centered at about 20°N and 20°S in the midbasin (similar to the SST pattern in Fig. 1a). The pattern for the coupled wind and SST anomalies are shown in Figs. 1a–c at day 2, day 30, and day 60, respectively. The most striking feature is a rapid propagation toward the equator. In two months, the disturbance has traveled more than 10° and starts to influence the equator. In addition, a westward propagation is also visible, especially in the vicinity of the equator. The characteristics of the wave propagation are the same as that discussed by LX (see

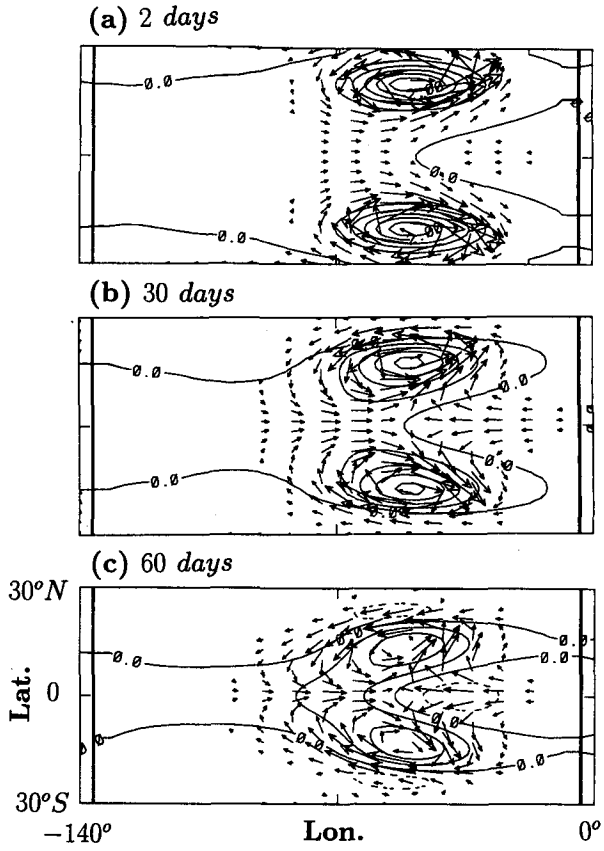

FIG. 1. The evolution of the coupled disturbances of SST (contour) and winds (arrows) with a basic state of a uniform easterly wind of 5 m s^{-1} (a) after 2 days, (b) after 30 days, and (c) after 60 days. The initial condition is a pair of elliptic-shaped SST anomalies centered at 20°N,S latitudes and −50° longitude [the shape is similar to the SST pattern in (a)]. The contour interval is 0.5 for SST. The maximum arrow is about 2 m s^{-1}. The figure shows clearly the rapid equatorward propagation and a tendency of westward propagation near the equator.

their Fig. 3a). The equatorward propagation can be understood as follows. A warm SST anomaly produces a westerly wind anomaly on its equator side because of the Coriolis force. This westerly wind anomaly reduces the mean trade wind and therefore causes warming on the equator side of the original warm anomaly. This causes the equatorward propagation of the warm anomaly. The addition of the BP effect improves the wind field significantly in the vicinity of the equator, where otherwise an excessive wind will be generated (see Fig. 9 of LX).

With the BP, the land-surface temperature can remotely affect the atmosphere over the ocean. Therefore, a simple land model is used to determine the land-surface temperature as

$$T = C_{PL} Q, \tag{2.4}$$

where C_{PL} is the coefficient that represents the land warming due to a unit solar radiation. A value of 5 K

$(100\ \mathrm{W\ m^{-2}})^{-1}$ seems to be not unreasonable. This value corresponds to a 5°C land warming under a solar radiation of 100 W m^{-2}. The land model here is mainly used to capture one essential feature of the land response: an instantaneous response to solar radiation. In addition, for simplicity, the Lindzen–Nigam model is also used over land. Of course, our results related to the land process should be taken cautiously. Nevertheless, sensitivity experiments suggest that in most cases, the land process does not affect our conclusion qualitatively. This is consistent with the finding of Li and Philander.

Equations (2.1)–(2.4) form a linear coupled ocean–atmosphere–land model. Some numerical aspects of the model are described as follows. The model is solved using a finite-difference scheme with a grid of 3° × 1°. For the atmosphere, a solid-wall boundary condition is imposed at the eastern and western boundary of the model domain. A radiation condition is set for the atmosphere at the northern and southern boundary of the model domain. A periodic eastern–western boundary condition and a solid wall northern–southern boundary condition are also tested and are found to produce no qualitative changes. The boundary condition for the ocean will be described where appropriate.

3. Modeling the annual cycle

In this section, a model domain of (−140°, 0°) × (20°S, 20°N) will be adopted. The basic state for SST, wind and mixed layer depth are shown in Figs. 2a–c respectively. Although crude, they capture some major features of the observed tropical Pacific: a cold tongue south of the equator, an easterly wind converging toward north of the equator, and a mixed layer deepening toward the west. In addition, the eastern coastline is tilted in the northwest–southeast orientation, simulating the coast in the eastern equatorial Pacific.

Following LX, an annual solar radiation is imposed, which has an amplitude increasing linearly from zero at the equator to 65 W m^{-2} at 20° of latitude (solid line Fig. 3a). The solar radiation reaches its maximum in January and June for the Southern and Northern Hemisphere, respectively (dotted line in Fig. 3a). Furthermore, since our interest is in the effect of the extratropical annual variability on the equator, the SST is prescribed similar to observations along the southern, eastern, and northern boundaries of the ocean (Figs. 3b–d). A no-heat-flux condition is imposed on the western boundary of the ocean. The prescription of boundary SSTs is to remedy the physical processes along the boundaries of our ocean model. The northern and southern boundary SST can to a large extent be produced locally by the annual solar radiation. However, our model lacks the coastal upwelling process along the eastern boundary, which has been shown important for the annual cycle (Philander and Pacanowski 1981). In addition, the coastal upwelling effect is also implied in the stronger annual variability in the easternmost part of the southern boundary. The prescribed boundary SST also makes it easier to compare with LX, in which the boundary SST plays an important role in determining the interior coupled variability.

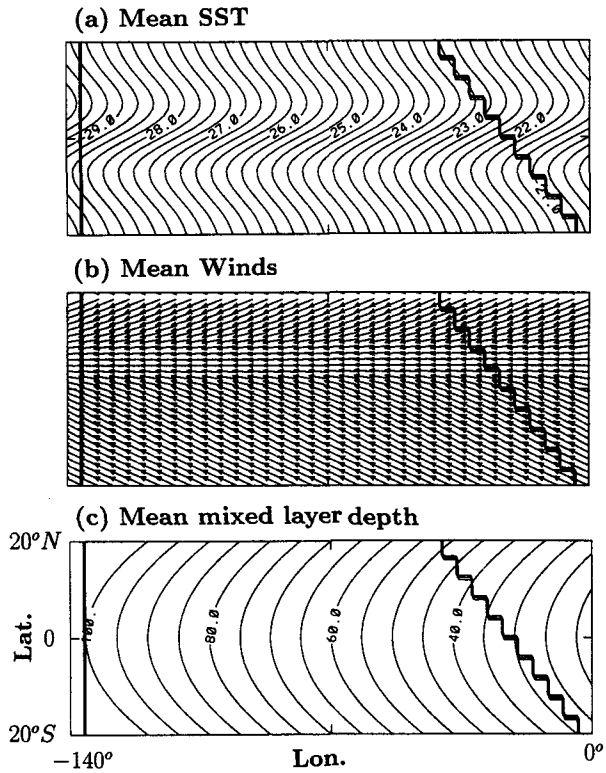

FIG. 2. The mean state of (a) SST, (b) winds, and (c) mixed-layer depth for the control run. The contour interval is 0.25°C for SST and 5 m for mixed-layer depth. The maximum arrow in (b) is about 5 m s^{-1}.

The control run is forced by the solar radiation in Fig. 3a, as well as all the boundary SSTs in Figs. 3b–d. The asymmetry that is necessary to generate annual variability on the equator comes from the mean state and the ocean geometry, as well as the boundary SST forcings. Figures 4a and 4b present the amplitude and phase of the SST, respectively. The model SST captures the major features of the observed SST (Fig. 1 of LX). The amplitude (Fig. 4a) shows a maximum variability tongue that extends from the east coast of the Southern Hemisphere northwestward toward the equator. The phase diagram (Fig. 4b) shows clearly the rapid propagation toward the northwest, reaching the equatorial region in about one to two months. On the land, the surface temperature is determined completely by the local radiation because of the land model (2.4).

Figure 5 shows a snapshot of SST (contour) and surface winds (vector) in boreal spring. The warm SST tongue along the equator has fully developed, with the

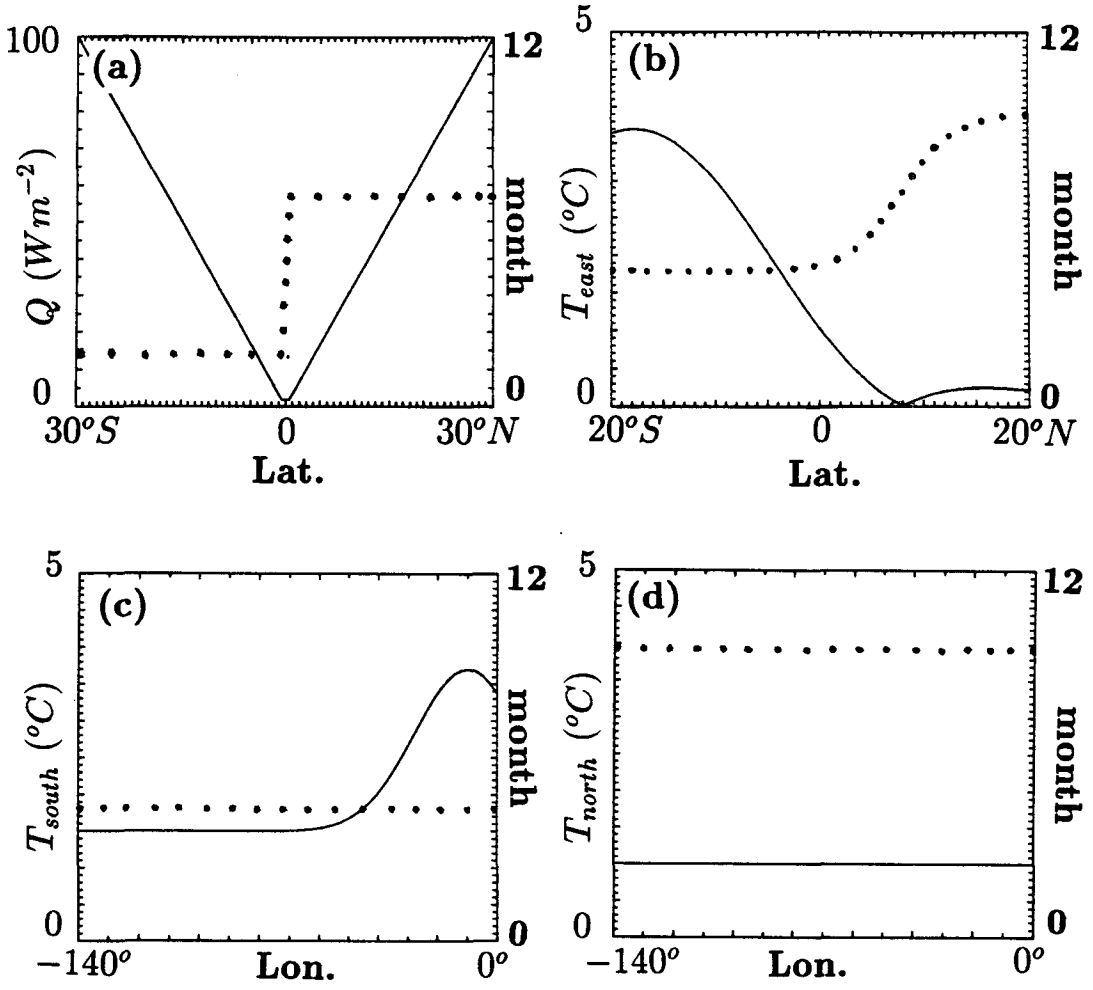

FIG. 3. The amplitude and phase of the radiation forcing and the boundary SST conditions for the control run. (a) Radiation heating as a function of latitude, (b) eastern boundary SST as a function of latitude, (c) southern boundary SST as a function of longitude, and (d) northern boundary SST as a function of longitude. Solid lines are amplitude and dashed lines are phase.

wind converging toward it. In contrast, on the land, the stronger heating over the Northern Hemisphere causes the southeast monsoon wind toward the inland.

The inclusion of BP improves our simulation significantly, especially near the equator. The most important improvement is the wind field in the vicinity of the equator. This can be seen by comparing Fig. 5 with the case without BP (Fig. 9 of LX). In the former, the wind field has a realistic amplitude at the order of 1 to 2 m s^{-1}, while in the latter the wind is one order of magnitude larger on the equator. This improvement is not unexpected because, as pointed out by Lindzen and Nigam, the BP effect suppresses the excessive wind convergence in the vicinity of the equator.

For a fixed SST anomaly, a shorter adjustment time τ forces a greater wind response on the equator. Thus, one should expect the coupled model to produce a stronger equatorial annual cycle. This is confirmed in Fig. 6, which plots the zonally averaged amplitude of annual harmonic for the control run (with τ = 1800 s) and two sensitivity experiments. Halving the adjustment time to τ = 900 s increases the annual variability on the equator significantly. To the contrary, doubling the adjustment time to τ = 3600 s reduces the annual variability.

The westward propagation along the equator is also improved significantly. One distinguished feature of the observed annual cycle on the equator is a westward propagation of both SST and zonal wind and a stationary response of the meridional wind (e.g., Fig. 15 of Chang and Philander 1994). This feature is simulated very well in our model as shown in Figs. 7a–c, which show the Hovmöller diagram of the model SST, zonal, and meridional winds along the equator. However, in the absence of BP, the model of LX shows a westward propagation for the SST and the zonal wind as well as

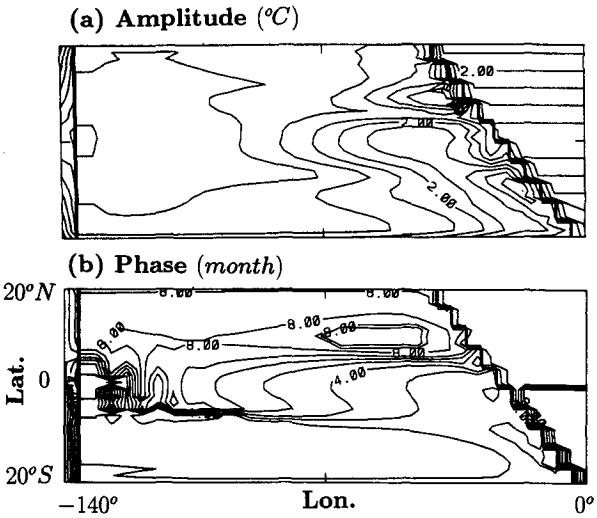

FIG. 4. The amplitude (CI = 0.5°) and phase (CI = 1 month) of the forced SST solution of the control run under the basic state in Fig. 2 and forced by the forcing in Fig. 3. The simulation captures the major features of the observed SST annual variability (Fig. 1 of LX). This includes a maximum variability tongue extending northwest toward the equator with a rapid phase propagation of about 1 to 2 months. The heavy line represents the coasts.

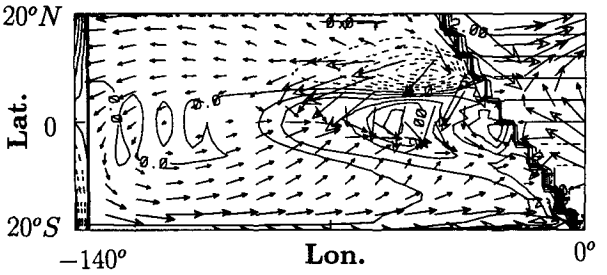

FIG. 5. One snapshot of the coupled anomalies of winds (arrows) and SST (contour) in boreal spring for the control run. The pattern is characterized by a strong warm tongue, and converging winds. The contour interval is 0.5°C for SST. The maximum wind is about 2 m s^{-1}.

the meridional wind (not shown) because all the signals propagate along the same characteristics. Thus, it is likely that the nonlocal response of the meridional wind on the equator is responsible for the quasi-stationary meridional annual variability along the equator.

To assess the role of various forcing components on annual variability, a set of experiments are performed. Figure 8 plots the amplitude of the annual harmonic for different cases. To evaluate the role of the wind evaporation–mixing mechanism, we repeat the control run but with a vanishing wind evaporation–mixing term in the SST Eq. (2.2). The response is shown in Fig. 8a. Compared with the control run in Fig. 4a, the annual variability is reduced dramatically, especially in the eastern equatorial ocean. The interior ocean is dominated by the local response to the solar radiation, which vanishes toward the equator due to the vanishing solar radiation and which decays westward due to the increase of the mixed layer depth. The boundary SST forcings are trapped almost entirely within the diffusive boundary layers along the southern, eastern and northern boundaries. This is caused by the lack of a propagation mechanism toward the equator and toward the west. Thus, we conclude that the wind evaporation–mixing mechanism and the associated propagation of coupled wave is crucial in producing the equatorial annual cycle in our model.

To evaluate the role of remote boundary SST forcings, we repeat the control run by suppressing the solar radiation. The amplitude of the annual variability in Fig. 8b shows a strong variability tongue in the eastern equatorial ocean. The overall resemblance between Fig. 8b and the control run in Fig. 4a shows that the remote effects from the extratropics as well as the eastern boundary are crucial for the equatorial annual cycle.

Furthermore, the southern boundary SST forcing is the most important. This can be seen in Figs. 8c and 8d, which show the amplitude of SST forced by the southern and eastern boundary SSTs respectively. Figure 8c shows that the southern boundary SST forces a substantial annual variability within the total boundary forcing case in Fig. 8b, especially farther away from the coast. The eastern boundary SST forcing can also force a significant annual variability but is mostly limited in about 30° of the east coast (Fig. 8d). Since the southern boundary SST represents the annual SST variability produced by the extratropical annual solar radiation there, our model annual cycle is forced by the extratropical annual variability, which propagates toward the equator from the Southern Hemisphere. This

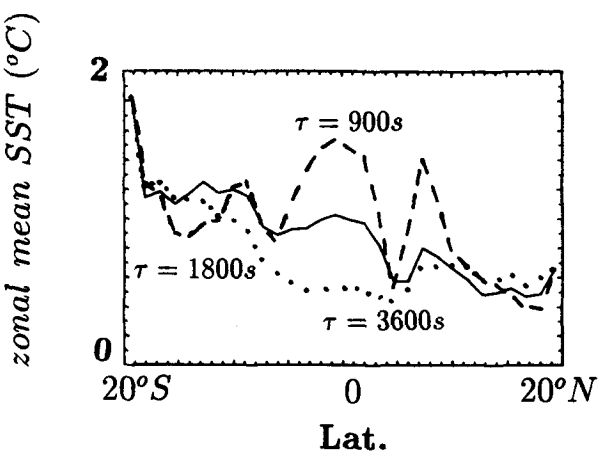

FIG. 6. The zonally integrated amplitude of the annual SST variability for three different "back-pressure" adjustment time: τ = 900, 1800, and 3600 s. A short adjustment time tends to enhance the annual variability in the equatorial band. This is caused by the stronger wind response in the Lindzen–Nigam model.

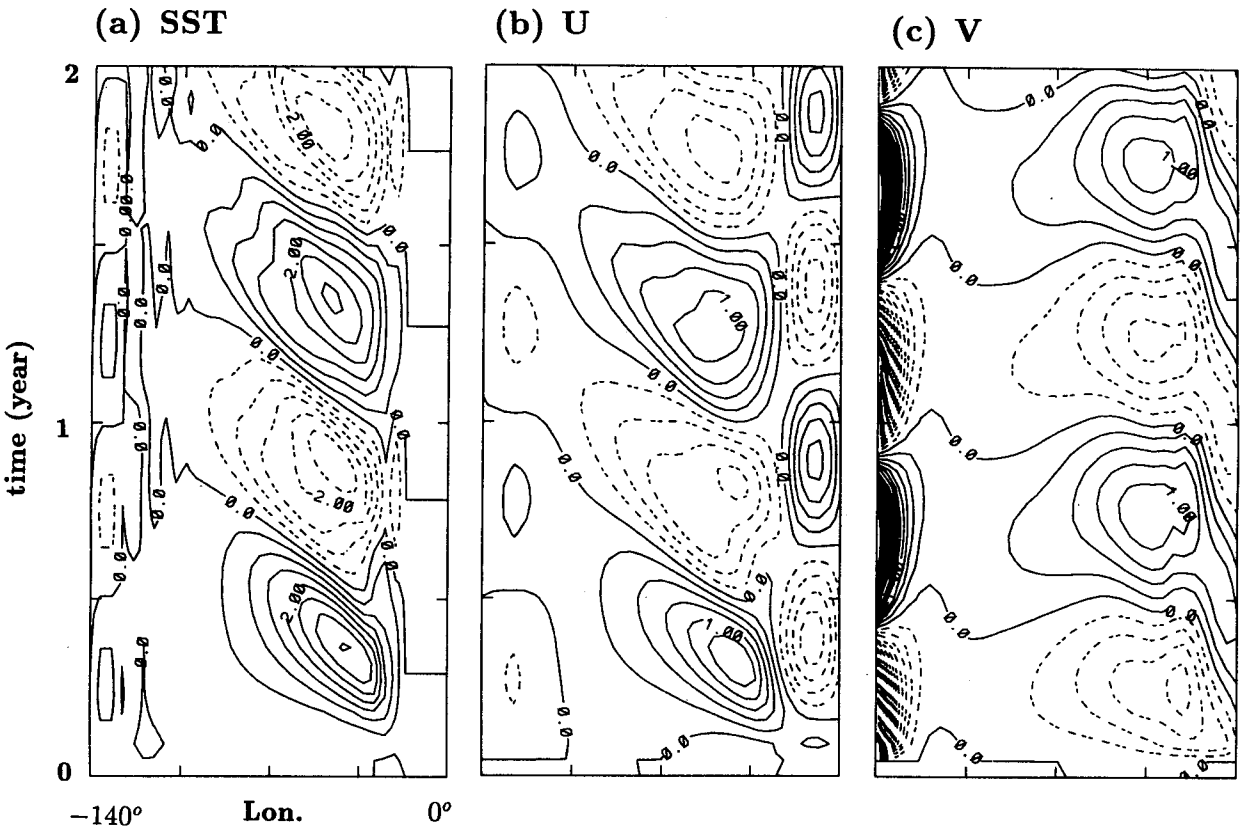

FIG. 7. The two-year Hovmöller diagram on the equator for (a) SST, (b) zonal wind U, and (c) meridional wind V. The contour interval is 0.5°C for SST and 0.25 m s^{-1} for U and V. The most important feature is a westward propagation of SST and U, but a quasi-stationary response of V. It was found that the mean wind-driven flow plays an important role in generating the different propagation characteristics.

conclusion remains true in other sensitivity experiments with various magnitudes of land response and for different coastline geometry.

4. Summary and discussions

This work presents so far the simplest model that simulates the two-dimensional spatial pattern of the complete annual cycle process under a given boundary SST forcing. It extends LX by including the "back-pressure" effect in the atmosphere. The key point is that most major features of the equatorial annual cycle can be understood in a linear framework as the equatorial forced response to the extratropical annual forcing. The extratropical annual solar radiation directly forces strong annual variability in the extratropics. In a coupled ocean–atmosphere system, this SST variability can propagate toward the equator through a coupled wave that is caused by the wind evaporation–mixing feedback. One feature that distinguishes this work (and LX) from others is our emphasis on the spatially broad annual variability as a single entity. It is our belief that a complete understanding of the equatorial annual variability should include its features not only on the equator but also away from the equator.

In an intermediate coupled model that is much more complete than ours, Li and Philander have found an enhancement of the annual cycle due to the evaporation effect. This is consistent with our results. It is likely that the evaporation enhancement can be explained by our mechanism. One should, however, keep in mind that our mechanism also include an additional effect of local wind mixing that is qualitatively similar to wind evaporation.

As demonstrated by Li and Philander, there are many factors that can enhance the equatorial annual cycle. This is also true in our model. The land effect can enhance the annual variability on the equator. This can be accomplished by either increasing the slope of the eastern boundary or by increasing the land-surface temperature response (C_{PL}) because both effects favor a stronger monsoon. Typically in our model, a doubling of the coastal slope or the land parameter C_{PL} enhance the amplitude of the annual variability on the equator by about 20% to 30%. Therefore, in our model, the land effect is important, but not dominant. This also seems to agree with the results of Li and Philander. However, in both works, both the land model and the atmosphere model over land are not very realistic. One therefore should be cautious about this conclusion.

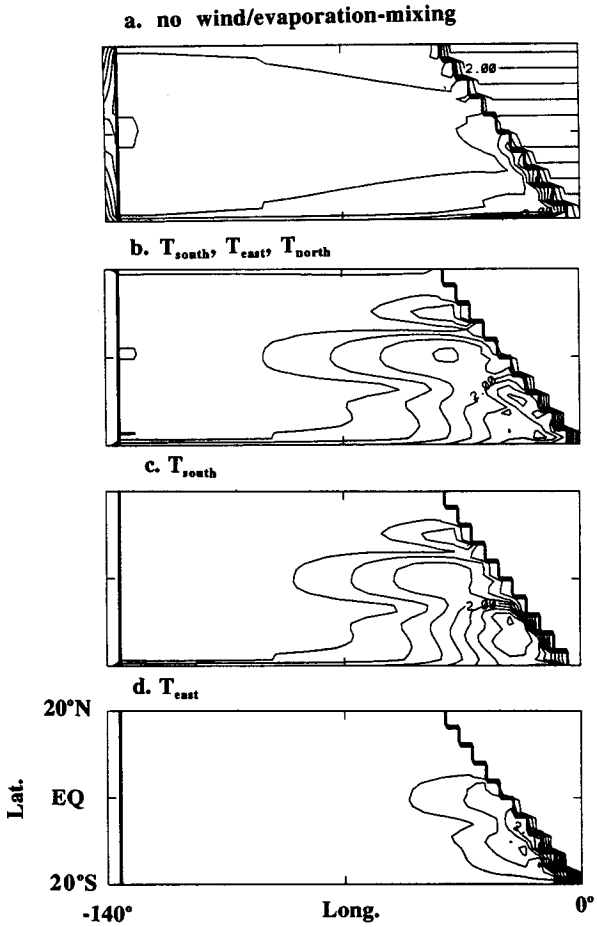

FIG. 8. The amplitude (contour interval 0.5°C) of the annual variability for sensitivity runs of control run in Fig. 4a. (a) The same as the control run, but without the wind-evaporation–mixing term in the SST equation. The equatorial annual variability is reduced dramatically. (b) The same as the control run but without the solar radiation forcing on the SST equation. The overall equatorial annual variability is reproduced very well. (c) The same as control but forced by the southern boundary SST forcing only. It produces the major part of the boundary-forced response in (b). (d) The same as the control run but forced by the eastern boundary SST only. The response mainly occurs near the shore. The figure shows that the wind evaporation–mixing term and the extratropical Southern Hemisphere annual variability play an important role in the equatorial annual cycle.

Including the upwelling effect proposed by Chang and Philander can also enhance the annual variability substantially. However, its effect is mainly limited within about 5° of the equator. This is determined by the nature of this upwelling instability, which is limited within the vicinity of the equator. However, as pointed out by Chang and Philander, the surface Ekman divergence can broaden the meridional extent of this mode substantially.

The stratiform cloud has been observed to be a crucial component of the equatorial annual variability (Klein and Hartmann 1993; Deser et al. 1993; Norris and Leovy 1994). This cloud effect can form a positive feedback with the SST: a colder SST is favorable for stratiform clouds, which increase albedo and therefore further cool the SST. In a crude approximation, this positive feedback can be added to our simple model by a reduction of the Newtonian damping of SST, as adopted by Li and Philander. This obviously increases the overall amplitude of the annual variability in our model.

The coastal upwelling effect is implied in our model. It has two important roles. The first is the production of the annual variability along the eastern coast. The second is the enhancement of annual variability in the easternmost part of the southern boundary. It seems that in our model the second effect plays a more important role for the overall structure of the equatorial annual cycle.

One will not be surprised if the real annual cycle is caused by a combination of various mechanisms. Fully coupled models have shown a considerable spread in the simulated annual cycle in the eastern equatorial Pacific (Mechoso et al. 1995). One explanation is that different models may capture different mechanisms. In contrast, the advantage and the purpose of using simple models, like the one in this paper, is that we can single out each mechanism and therefore understand it. This is clearly important for us to understand what happened in the fully coupled models. However, a simple model may have a built-in bias against other mechanisms. Therefore, it is our belief that one should always be careful in assessing the relative importance of different mechanisms in the real world solely based on a simple model.

Finally, the wind evaporation–mixing feedback can also be understood from another viewpoint. The coupled system Eqs. (2.1)–(2.4) has free modes in the absence of forcing. If we only retain the evaporation term and the local variability term in the SST Eq. (2.2), the coupled mode will be caused solely by the wind-evaporation–mixing feedback, and the resulted free mode will be called the wind evaporation–mixing mode. In the absence of BP, this mode has been shown analytically in LX as a nondispersive SST mode (Neelin 1991) that propagates toward the equator. With the BP, the free mode can be solved numerically after including the diffusion term similar to Chang and Philander. One example is shown in Fig. 9 under a symmetric basic state that is the same as in Fig. 1. The rapid equatorward propagation feature is clear. It is interesting to compare the wind evaporation–mixing mode with the upwelling mode of Chang and Philander. For both modes, the most unstable mode is antisymmetric (in the presence of symmetric basic state). However, the wind evaporation–mixing mode is weakly unstable[1] but with high frequency (months). While the up-

[1] The instability is caused by the asymmetric, nonlocal atmospheric response to the SST anomaly, which in turn is caused by the variation

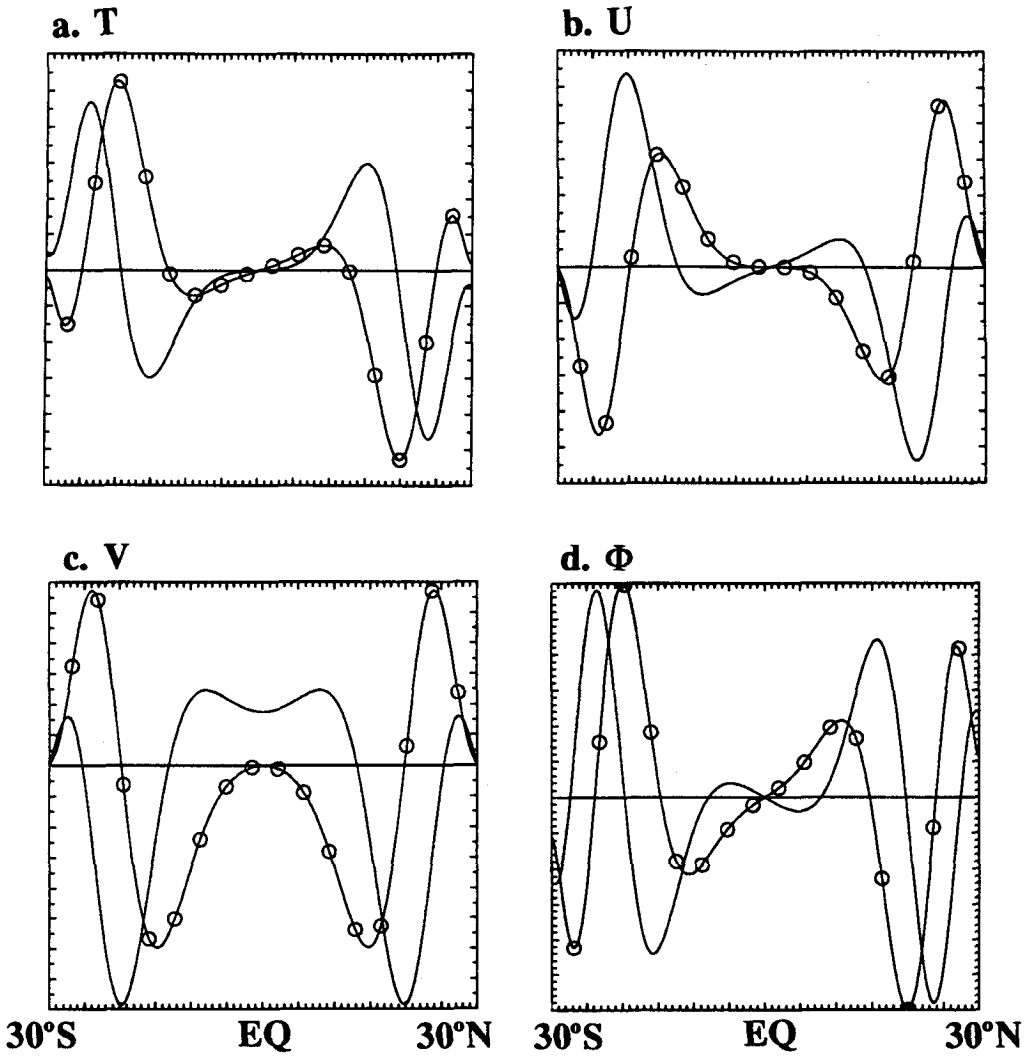

FIG. 9. One example of the eigenfunctions of (a) SST, (b) zonal wind, (c) meridional wind, and (d) geopotential height for the wind evaporation–mixing mode in the case of zonal wavenumber 0 case. In addition to the local variability and diffusion terms, the only term that remains in the SST Eq. (2.2) is the wind-evaporation–mixing term. Other model parameters and basic state are the same as in Fig. 1. The mode plotted is the most unstable mode. In each panel, the circled curve lags the solid curve by 90°. The eigenvalue problem is solved by finite differencing with solid boundary condition ($V = 0$) and no-heat-flux condition ($\partial_x T = 0$) on the northern–southern boundaries. In dimensional form, the eigenvalue has the real and imaginary parts as about 1/(10 months) and 1/(1 month), respectively.

welling mode has a strong growth rate, it is almost stationary on the equator (in the absence of advection). For the wind evaporation–mixing mode, the most unstable waves are nearly nondispersive. Thus, the high-frequency nature of the wind evaporation–mixing mode produces a rapid equatorward propagation in both its phase and group velocity (not shown) that are similar to the case without BP in LX. It is this fast equatorward propagation nature of the wind evaporation–mixing mode that carries the annual signal toward the equator.

Acknowledgments. The author thanks the three reviewers for helpful comments. Ms. Y. Sun has per-

of the Coriolis parameter. With BP, the atmospheric response is always stronger on the equatorial side of the anomaly because of the smaller Coriolis force. Thus, a symmetric SST warm anomaly will produce a westerly wind on top of the maximum SST that is the same as on the equatorial side. With a mean easterly wind, the former causes the unstable growth of the SST anomaly, while the latter causes the propagation toward the equator. The instability disappears in the absence of BP (as in LX) because the wind response to the SST gradient is local and therefore is zero right above SST maximum. A discussion with a box model has been presented by Xie (1996).

formed the eigenvalue problem calculation in Fig. 9. This work is supported by PACS/NOAA and Climate Dynamics/NSF.

REFERENCES

Chang, P., and S. G. H. Philander, 1994: A coupled ocean–atmosphere instability of relevance to the seasonal cycle. *J. Atmos. Sci.,* **51,** 3627–3648.

——, B. Wang, T. Li, and L. Ji, 1994: Interactions between the seasonal cycle and the Southern Oscillation—frequency entrainment and chaos in an intermediate coupled ocean–atmosphere model. *Geophys. Res. Lett.,* **21,** 2817–2820.

Deser, C., J. J. Bates, and S. Wahl, 1993: The influence of sea surface temperature gradients on stratiform cloudiness along the equatorial front in the Pacific Ocean. *J. Climate,* **6,** 1172–1180.

Horel, J. D., 1982: On the annual cycle of the tropical Pacific atmosphere and ocean. *Mon. Wea. Rev.,* **110,** 1863–1878.

Jin, F. F., J. D. Neelin, and M. Ghil, 1994: El Niño and the Devil's staircase; annual subharmonic steps to chaos. *Nature,* **264,** 70–72.

Klein, S. A., and D. L. Hartmann, 1993: The seasonal cycle of low stratiform clouds. *J. Climate,* **6,** 1587–1606.

Lindzen, R., and S. Nigam, 1987: On the role of sea surface temperature gradients in forcing low-level winds and convergence in the Tropics. *J. Atmos. Sci.,* **44,** 2418–2436.

Liu, Z., and S. P. Xie, 1994: Equatorward propagation of coupled air-sea disturbances with application to the annual cycle of the eastern tropical Pacific. *J. Atmos. Sci.,* **51,** 3807–3822.

Mechoso, C. R., and Coauthors, 1995: The seasonal cycle over the tropical Pacific in coupled ocean–atmosphere general circulation models. *Mon. Wea. Rev.,* **123,** 2825–2838.

Mitchell, T. P., and J. M. Wallace, 1992: Annual cycle in equatorial convection and sea surface temperature. *J. Climate,* **5,** 1140–1152.

Neelin, J. D., 1989: On the interpretation of the Gill model. *J. Atmos. Sci.,* **46,** 2466–2468.

——, 1991: The slow sea surface temperature mode and the fast-wave limit: Analytic theory for tropical interannual oscillations and experiments in a hybrid coupled model. *J. Atmos. Sci.,* **48,** 584–606.

Norris, J. R., and C. B. Leovy, 1994: Interannual variability in stratiform cloudiness and sea surface temperature. *J. Climate,* **7,** 1915–1925.

Philander, S. G. H., and R. C. Pacanowski, 1981: The oceanic response to cross-equatorial winds (with application to coastal upwelling in low latitudes). *Tellus,* **33,** 201–210.

Reed, R. K., 1977: On estimating insolation over the ocean. *J. Phys. Oceanogr.,* **7,** 482–485.

Suarez, M. J., and P. S., Schopf, 1988: A delayed oscillator for ENSO. *J. Atmos. Sci.,* **45,** 3282–3287.

Tziperman, E., L. Stone, M. Cane, and H. Jarosh, 1994: El Nino chaos: Overlapping of resonances between the seasonal cycle and the Pacific ocean-atmosphere oscillator. *Science,* **264,** 72–74.

Wang, B., 1994: On the annual cycle in the tropical eastern central Pacific. *J. Climate,* **7,** 1926–1942.

Xie, S-P., 1994: Oceanic response to the wind forcing associated with the intertropical convergence zone in the Northern Hemisphere. *J. Geophys. Res.,* **99,** 20 393–20 402.

——, 1996: Unstable transition of the tropical climate to an equatorially asymmetric state in a coupled ocean–atmosphere model. *Mon. Wea. Rev.,* in press.